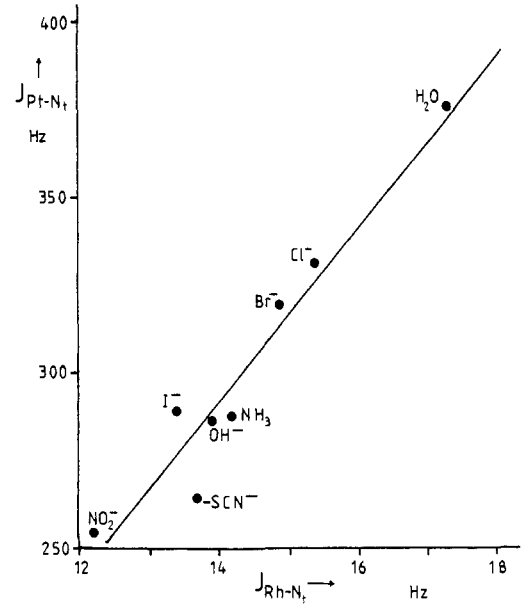

Figure 2. Plot of $J(Pt-N_t)$ in the series $Pt(NH_3)_3Z^{m+}$ (**1**) against $J(Rh-N_t)$ in the series $Rh(NH_3)_5Z^{m+}$ (**3**). The line shown is the line of best fit, $J(Pt-N_t) = 25.07[J(Rh-N_t)] - 59.7$.

sensitive primarily to the effect of Z on the platinum 6s contribution to the $Pt-N_t$ bond,[8] an approach that has previously successfully rationalized the variations in one-bond coupling constants between ^{195}Pt and ^1H, ^{31}P, and ^{13}C.[12-15] Basch et al.[16] have since studied the bonding in the hypothetical molecule *cis*-$Pt(NH_3)_2(CH_2OH)(OCH_3)$ (a model for the ascorbic acid C,O-chelate complex). They concluded that the platinum $5d_{x^2-y^2}$ orbital made the largest contribution to the Pt–N bonds and that this contribution was dramatically reduced in the Pt–N bond trans to carbon. Our qualitative discussion of NMR parameters is in accord with their findings. If the metal s orbital makes only a relatively small contribution to the metal–nitrogen bonds, and coupling constants are sensitive primarily to this contribution, care must be taken to avoid facile attempts to use these coupling constants alone as a measure of bond strength.

From the correlations noted above, it is clear that NMR parameters for N_t in the rhodium complexes are affected by Z in a way similar to those for N_t in the platinum complexes, and conditions i–iii given as desirable in the Introduction do apply. The usual method for characterizing rhodium(III) compounds in solution is by visible–UV spectroscopy, and this method must continue to be useful. However, the broadness of the peaks can make it difficult to be certain about the presence of minor components in a solution, especially if the different ligands present occupy similar positions in the spectrochemical series. The ^{15}N NMR lines are very sharp, and there is little probability that two different species would have identical chemical shifts and Rh–N coupling constants for all of the ammine ligands present. Even relatively minor components of a mixture may be detected and characterized.

Acknowledgment. We are grateful for financial support from a University of Queensland Special Project Grant and the Australian Research Grants Scheme.

Registry No. $[Rh(NH_3)_5Cl]Cl_2$, 13820-95-6; $[Rh(NH_3)_5Cl](NO_3)_2$, 21264-83-5; $[Rh(NH_3)_5(ONO_2)](NO_3)_2$, 41762-28-1; $[Rh(NH_3)_5Br]Br_2$, 19682-70-3; $[Rh(NH_3)_5I]I_2$, 32088-27-0; $[Rh(NH_3)_5I](NO_3)_2$, 15337-81-2; $[Rh(NH_3)_6](ClO_4)_3$, 16786-63-3; *trans*-$[Rh(NH_3)_4(SO_3)(CN)]\cdot 2H_2O$, 117064-14-9; *trans*-$[Rh(NH_3)_4(CN)(H_2O)]Cl_2$, 116971-76-7; $[Rh(NH_3)_5(CN)]Cl_2$, 22653-47-0; $[Rh(NH_3)_5(H_2O)](ClO_4)_3$, 15611-81-1; $[Rh(NH_3)_5(NCO)](ClO_4)_2$, 69308-81-2; $[Rh(NH_3)_5(NCS)](ClO_4)_2$, 15244-72-1; $[Rh(NH_3)_5(SCN)](ClO_4)_2$, 15244-73-2; *trans*-$Na[Rh(NH_3)_4(SO_3)_2]$, 117064-15-0; $[Rh(^{15}NH_3)_5Cl]Cl_2$, 116971-77-8; $[Rh(^{15}NH_3)_5Cl](NO_3)_2$, 116996-18-0; $[Rh(^{15}NH_3)_5Br]Br_2$, 116971-78-9; $[Rh(^{15}NH_3)_5I]I_2$, 116971-79-0; $[Rh(^{15}NH_3)_6](ClO_4)_3$, 116971-81-4; *trans*-$[Rh(^{15}NH_3)_4(SO_3)(CN)]\cdot 2H_2O$, 116971-82-5; *trans*-$[Rh(^{15}NH_3)_4(CN)(H_2O)]Cl_2$, 116971-83-6; $[Rh(^{15}NH_3)_5(CN)]Cl_2$, 116971-84-7; $[Rh(NH_3)_5(OH)]^{2+}$, 26214-91-5; $[Rh(NH_3)_5(ONO)]^{2+}$, 34412-16-3; $[Rh(NH_3)_5(NO_2)]^{2+}$, 34412-13-0; $[Rh(^{15}NH_3)_5(H_2O)](ClO_4)_3$, 116996-83-9; *trans*-$Na[Rh(^{15}NH_3)_4(SO_3)_2]$, 116971-85-8.

Supplementary Material Available: Experimental details of compound preparation and Table II, containing microanalytical data (8 pages). Ordering information is given on any current masthead page.

(12) Appleton, T. G.; Clark, H. C.; Manzer, L. E. *Coord. Chem. Rev.* **1973**, *10*, 335.
(13) Pidcock, A.; Richards, R. E.; Venanzi, L. M. *J. Chem. Soc. A* **1966**, 1707.
(14) Appleton, T. G.; Bennett, M. A. *Inorg. Chem.* **1978**, *17*, 738.
(15) Chisholm, M. H.; Clark, H. C.; Manzer, L. E.; Stothers, J. B.; Ward, J. E. H. *J. Am. Chem. Soc.* **1973**, *95*, 8574.
(16) Basch, H.; Krauss, M.; Stevens, W. J. *Inorg. Chem.* **1986**, *25*, 4777.

Contribution from the Department of Chemistry, The University of Chicago, Chicago, Illinois 60637

CrB_4 and MnB_4: Electronic Structures of Two Unusual Systems Containing the Tetragonal Carbon Net

Jeremy K. Burdett* and Enric Canadell†

Received July 16, 1987

It is shown how the tetragonal carbon structure, quite energetically unfavorable for an electron count appropriate for carbon, may be stabilized by removal of electrons by a suitable metal. This observation is understandable by using a result from the method of moments. CrB_4 that contains a boron net of this type appears optimal not only from the viewpoint of the stability of this non-metal framework but also from that of the metal coordination. For MnB_4, Mn–B and Mn–Mn antibonding orbitals are occupied, the non-metal electron density is larger than for chromium, and the structure distorts as a result of coupling between the desires of metal coordination and that of the nonmetal array. For M = Fe, Co, and Ni the tetragonal carbon lattice is so destabilized as a result of the higher electron count that it may well be unstable. CrB_4 phases with these metals are not known.

I. Introduction

There are several metal borides and related species that may be visualized in geometric terms as arising via the insertion of a metal atom into a network of non-metal atoms. Perhaps the best known example is the structure of CaB_6, where Longuet-Higgins and Roberts showed[1] many years ago that the two electrons donated by the calcium atom satisfy exactly the bonding requirements of the vertex-linked boron octahedra. The structures of $CaSi_2$ and $CaIn_2$ have a similar attraction for electron counting.[2]

† Present address: Laboratoire de Chimie Théorique, Université de Paris Sud, 91405 Orsay, France.

(1) Longuet-Higgins, H. C.; Roberts, M. de V *Proc. R. Soc. London* **1954**, *A224*, 336.

0020-1669/88/1327-4437$01.50/0

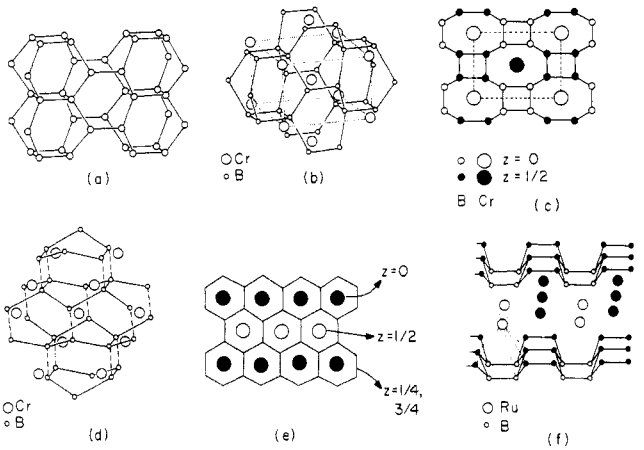

Figure 1. (a) Perspective view of the tetragonal carbon structure. (b) Perspective view of the CrB_4 structure. (c) CrB_4 structure projected on (0, 0, 1). (d) Perspective of structure c showing its construction from corrugated 6^3 sheets of boron atoms. (e) Projection viewed down on a single sheet of a defect puckered AlB_2 type of structure of MB_4 stoichiometry. The open and closed circles represent the occupied sites of alternate layers. (f) Perspective view of the RuB_2 structure.

Table I. Interatomic Separations in CrB_4 and MnB_4 (Å)

	CrB_4	MnB_4
M–B (square)	2.067 (×4)	2.062 (×4)
M–B (cube)	2.268 (×8)	2.189 (×4)
		2.210 (×4)
mean	2.201	2.154
B–B (square)	1.662	1.669
	1.693	1.825
B–B (intersquare)	1.911 (×2)	1.839
		1.871
mean	1.794	1.801
M–M	2.866	2.949

The former consists of arsenic-like puckered sheets of silicon atoms (Si^- is isoelectronic with arsenic). $CaIn_2$ consists of a hexagonal diamond cage of In atoms. In this case In^- is isoelectronic with carbon. In each example the electropositive metal occupies a well-defined interstice in the lattice.

The systems described in this paper appear geometrically to fit into this pattern but, as we shall see, are electronically quite different. We will present a discussion based upon orbital ideas supported by numerical results from molecular orbital calculations on fragments of the structure and band structure computations using the tight-binding method for crystalline solids, which both use the extended Hückel method.

II. Structures of CrB_4 and MnB_4

The structures of CrB_4 and MnB_4 are based[3,4] upon a lattice, the tetragonal carbon structure, which, unlike those for $CaSi_2$ and $CaIn_2$, is unknown as a homoatomic metal-free system. A derivative arrangement, however, is known for β-BeO, and some ternary oxides, such as $LiAlO_2$, are also found in this structure type. The geometrical arrangement is shown in Figure 1a. It consists of squares of non-metal atoms that are linked into a three-dimensional arrangement in the manner shown. CrB_4 adopts a distorted, stuffed version of this arrangement and is orthorhombic (*Immm*) with the boron atoms in 8(j) and the metal atoms in 2(a).[3] The structure is shown in Figure 1b. The "squares" in the structure are not exactly regular. There is a slight rectangular distortion leading to different B–B distances (Table I). However, it is reported that this difference is not satistically significant.[3] The net is clearly a distortion of the "ideal" structure, which would have tetragonal symmetry. The metal atoms lie in the same plane and between these squares of atoms to give chains of the type shown in **1**, which lie along the *b* axis of the unit cell. The

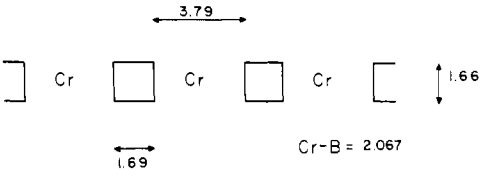

1

three-dimensional structure may be built up by stacking units of this type on top of each other shifted by $(a + b)/2$ relative to the chain below. These chains are linked above and below by B–B bonds, which complete four-coordination at each center. The metal atoms are now in a rather distorted twelve-coordinate boron environment. In the plane of the chain there are four Cr–B distances of 2.06 Å (**1**) to the boron atoms in a rectangularly distorted square. Above and below this chain there are analogous units that provide eight close boron atoms (2.26 Å) as shown in **2**.

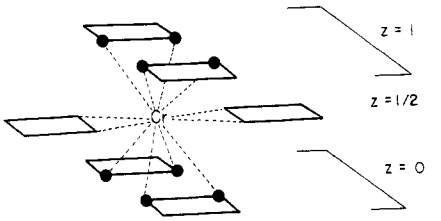

2

These atoms are arranged at the vertices of a cube that has been distorted to a rectangular prism. The distortion of both the square and the cube are considerable, but these geometric labels are useful descriptors. (Another way to view the coordination with special reference to Figure 1d is as a distorted hexagonal prism.) Further away from the central metal atom of **2** are two more metal atoms, which lie along *z* and complete the coordination environment of the metal. The Cr–Cr distance is not particularly short (Table I), but we note that it is similar to the Mn–Mn distance in $Mn_2(CO)_{10}$ of 2.94 Å, where two Mn atoms are linked by a single metal–metal bond.

The structure of MnB_4 is similar to the one described for CrB_4, but here the B_4 "squares" are considerably distorted with distances of 1.67 and 1.83 Å. (The quality of the data[4] is such, however, that this difference may not be very significant, but more about this later.) The Mn–Mn distance has increased (Table I) compared to that for the chromium case, and the metal atoms and the "square" boron atoms are slightly nonplanar, so that the M–B distances to the cubal atoms are now not all equal. Another way of looking at these structures that will be useful to us later is shown in Figure 1d and emphasizes the assembly of the solid from corrugated graphite-like 6^3 sheets of boron atoms. Two of the linkages in the squares are those that link these sheets together. In fact we could describe the structure (Figure 1e) as a defect AlB_2 structure (to give the MB_4 stoichiometry) with the sheets puckered and linked together. (The metal coordination in AlB_2 is a hexagonal prism of boron atoms. Compare this with our description above of the metal coordination in CrB_4.) A different linking of similar sheets occurs in the stable structure of elemental gallium. Another interesting relationship is that of CrB_4 to the RuB_2 structure shown in Figure 1f. By comparison with Figure 1b, the non-metal net of RuB_2 is just a broken-up form of tetragonal carbon, followed by a slippage of the sheets with respect to each other. The distortion found in MnB_4 is toward a separation of these corrugated sheets. Given that increasing electron count often leads to broken-up structures (see for example ref 5), we are encouraged to look for an electronic explanation of this observation.

(2) See for example: (a) Pearson, W. B. *The Crystal Chemistry and Physics of Metals and Alloys*; Wiley: New York, 1972. (b) Lytle, W. H. M. S. Thesis, Arizona State University, 1982.
(3) Andersson, S.; Lundstrom, T. *Acta Chem. Scand.* **1968**, *22*, 3103.
(4) Andersson, S.; Carlsson, J.-O. *Acta Chem. Scand.* **1970**, *24*, 1791.
(5) Burdett, J. K. *Nature (London)* **1979**, *279*, 121.

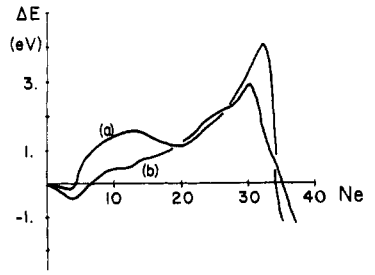

Figure 2. Variation in stability of the "tetragonal boron" structure (the non-metal net of the real CrB_4 arrangement) relative to (a) the cubic diamond structure and (b) the "ideal" tetragonal carbon structure, as a function of the number of electrons per unit cell (eight atoms). The half-full situation (i.e., elemental carbon) corresponds to 32 electrons. A negative value indicates that the actual tetragonal boron structure is more stable.

One of the interesting observations concerning the MB_4 structures is that the phase has not been made with any metals other than Cr and Mn. Experiments have been performed with V, Fe, Co, and Ni. Stable phases do exist of course for other metals with this stoichiometry but with different structure, Y being an example.

III. Electronic Structure of Tetragonal Carbon

First we shall be interested in viewing the stability of the non-metal net alone. To this end we have performed tight-binding band structure calculations on the tetragonal carbon structure using the parameters given in the Appendix. The computed density of states plot is very similar to that for cubic diamond, and the electronic situation is shown schematically in **3**. A band gap

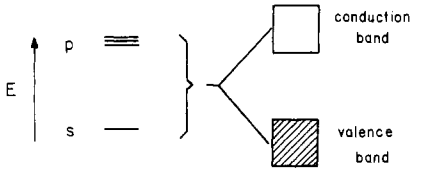

3

appears at the Fermi level (four electrons per atom) that separates the valence and conduction bands of these tetrahedrally coordinated systems. The computed band gap and location of the Fermi level in the two arrangements are very similar, but the tetragonal carbon structure is found to be quite unstable with respect to the observed cubic allotrope by 0.51 eV per carbon atom.[6] The electronic reasons for this are 2-fold. First, the ring strain energy introduced by the presence of 90° angles at carbon is considerable, and second, as we have recently shown,[7] the presence of four-membered rings is energetically extremely unfavorable for systems with a half-filled band of electrons from "topological" considerations. Six-membered rings (as in cubic diamond), however, are stable on both counts at the half-filled band. These two effects combine to produce an energetically unfavorable carbon arrangement. For electron counts other than four per atom (the half-filled band) the results are somewhat different.

Figure 2a shows a computed energy difference curve, which compares the stability of the non-metal net in CrB_4 with that of the diamond structure as a function of the electron count. The results correspond to a boron lattice. Since calculations of the type we have employed here are not reliable when estimating energy changes associated with bond length variations, in all these computations we have kept the average B–B distance constant during the distortion. This is an attempt to keep the second moment of the density of states fixed to allow us to see more clearly what is going on. Past the half-filled band the computed energy differences of Figure 2 become enormous and unrealistic and are therefore not shown. This is a direct result of using parameters for carbon and boron that lead to large interatomic overlap and strongly destablized antibonding orbitals. For real species with these electron counts, oxygen- and fluorine-containing species for example, the overlap is much smaller, and such instabilities will not occur of course. The most important result from the calculation is that with lower or higher electron counts than for carbon itself the energetic penalty associated with the tetragonal structure decreases. This is a result similar to the one we have reported before[7] for the energy difference curve as a function of band filling for the two structures supercubane and cubic diamond. The former is a hypothetical structure containing vertex-linked cubes of atoms, which is also destabilized at the carbon electron count by the large number of squares in the structure. For the supercubane example, however, a definite stability field was computed at the low band filling. In this plot the stability field with respect to the real tetragonal boron structure is a shallow one but is larger with respect to the "ideal" geometry (vide infra).

These energy difference curves have been interpreted as arising via a difference in the fourth moment of their energy density of states, with use of the language of the method of moments.[8,9] An energy difference curve controlled by a fourth-moment difference has one crossing between the empty and half-full band fillings. These moments may be related in turn to the number of returning walks of the same length through the lattice. In the present case a closed walk of length 4 around the squares of atoms in the CrB_4 structure, absent in the cubic diamond arrangement, is particularly important. We will present energy difference curves as a function of electron count even though we only have two experimental points to compare (CrB_4, MnB_4). The *shape* of the overall curve gives us vital clues as to the factors influencing the strutural problem.

If such 4-walks are important in influencing the stability of these structures, weakening their effect by examining a structure where all B–B distances are set equal at 1.80 Å (cf. Table I) should be instructive. This is the "ideal" tetragonal carbon net (with geometric details given in the Appendix), and its energetic comparison with the non-metal net observed in CrB_4 is shown in Figure 2b. This is a typical fourth-moment problem.[8,9] The "ideal" structure with its longer distances within the four-membered ring and hence smaller fourth moment is energetically unfavorable early in the band filling but much more favorable later on with maximum stability near the half-filled band at about 30 electrons per eight-atom unit cell. Both of these plots show, however, that the diamond and "ideal" tetragonal carbon structures are more stable at 24 electrons (the electron count appropriate for elemental boron in this structure) than the observed structure of the non-metal net in CrB_4.

A comment is due at this stage concerning the observation of the derivative tetragonal carbon structure for the β phase of BeO. One way of stabilizing a structure containing four-membered rings at the half-filled point is to substitute the lattice alternately with atoms of different electronegativities. This is just the case in β-BeO. We discuss this problem in general elsewhere.[9]

What can we conclude from these results? One result is that, in contrast to the structures where electron donation *to* the lattice produces an electronically stable network of four-connected atoms with four electrons per atom, the homoatomic tetragonal carbon structure may only be energetically accessible by ensuring that the electron count avoids four electrons per atom. Specifically for the tetragonal boron analogue, we wish not to transfer electron density to the non-metal net on insertion of the metal. This is somewhat at variance with present ideas concerning electron transfer in metal borides in general. Since boron-rich species are common among the rare earths and early transition metals but rare among the electronegative late transition metals, it is usually supposed that, in the systems with stoichiometry MB_2 to MB_{12}, electron transfer occurs from metal to boron. In systems with

(6) The solid-state language here could appear confusing. The structure type is the "tetragonal carbon" one, but it is boron atoms that occupy the lattice sites in these computations.
(7) Burdett, J. K.; Lee, S. *J. Am. Chem. Soc.* **1985**, *107*, 3063.
(8) Burdett, J. K.; Lee, S. *J. Am. Chem. Soc.* **1985**, *107*, 3050.
(9) Burdett, J. K. *Struct. Bonding (Berlin)* **1987**, *65*, 29.

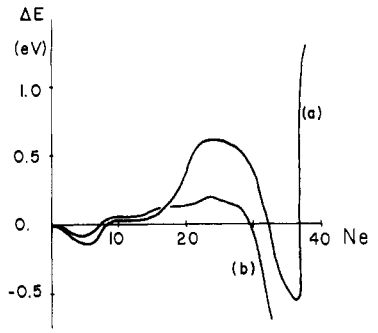

Figure 3. Variation in stability of the "tetragonal boron" structure (the non-metal net of the real CrB_4 arrangement) relative to (a) the non-metal net of the real MnB_4 structure and (b) the "semi-MnB_4" structure via a distortion that maintains orthorhombic symmetry and is less extreme than that of (a). See the Appendix for details. A negative value indicates that the actual tetragonal boron structure is more stable.

a smaller boron content than MB_2 the converse is supposed. The present pair of species, the only examples of their type, do not fit in with such a general approach.

Perhaps the more interesting distortion of the net is the one associated with the distortion of the non-metal net from CrB_4 to MnB_4. Figure 3a shows a computed energy difference curve for this possibility. In addition in Figure 3b we show the results of computations on the "semi-MnB_4" distortion. This is a structure which preserves the orthorhombic space group but contains a smaller rectangular distortion of the squares than that found in MnB_4 itself. The details are given in the Appendix. As before, the average B–B distance was kept constant during each distortion. For electron counts past the half-filled band (32 electrons) the amplitude starts to get very large, in a way similar to that of Figure 2, and the results are not very meaningful.

To avoid this problem, we can perform a Hückel calculation on the parent and distorted structures. (This is an "extended Hückel" calculation, but with overlap dropped in the off-diagonal elements of the Hamiltonian matrix. It is not restricted, however, to interactions between neighboring atoms as in a "true Hückel" calculation.) **4** shows the result for the "semi-MnB_4" distortion.

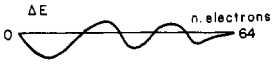

4

The energy difference curve is very similar to the extended Hückel computation of Figure 3b for less than the half-full band. The result is clearly, in the language of moments, a sixth-moment problem. The system with the larger sixth moment is the undistorted CrB_4 net and is the structure more stable for low band fillings. How this actually occurs is shown in **5**–**7**. (See Figure

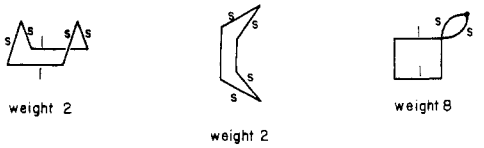

5 **6** **7**

1 for the location of these six-membered rings.) The distortion involves not only a bond-length-conserving rectangular distortion at each boron center but also changes in the bond lengths of the six-membered rings **5** and **6** and the 6-walks of **7**. These, when weighted, show a larger sixth moment for the CrB_4 net than for the MnB_4 net. In **5**–**7** l indicates a linkage that lengthens on distortion and s one that shortens during the distortion. Shorter contacts have larger overlap integrals and hence larger weights in the 6-walk, which contributes to the sixth-moment difference. It is difficult and probably not very rewarding to evaluate all the numerical contributions to the walks and hence moments of different order in this changing bond length problem, and it is not clear either that the walks of **5**–**7** are the dominant ones.

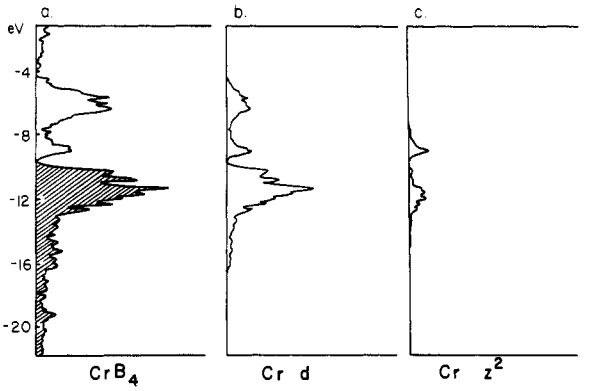

Figure 4. Density of states for (a) CrB_4 and for projections of the (b) Cr 3d and (c) Cr z^2 orbitals. The shading in (a) corresponds to the occupied levels for CrB_4.

However, what is clear from the plot of **4** is that this is a sixth-moment problem.

The results of this section are interesting ones. The tetragonal structure of the non-metal atoms found in CrB_4 is energetically quite unfavorable for an all-carbon net but becomes less disfavored for smaller or higher electron counts. Relative to the cubic diamond structure, the tetragonal structure is energetically disfavored by half as much at the boron electron count compared to that for carbon (Figure 2). Clearly, removal of electron density from the non-metal net by addition of a suitable species will stabilize this tetragonal net even more. The observed geometry of the non-metal net should also distort to the "ideal" structure for these electron counts, and the distortion to the net found in the MnB_4 structure is also computed to be favored for 20–30 electrons per cell. Distortions in these MB_4 structures will of course, in practice, be limited by the requirements of the metal–boron and metal–metal interactions, which we examine below.

IV. Electronic Structure of CrB_4

Whereas the atomic energy levels of the free metal atom in CaB_6 lie to much higher energy than the atomic boron levels, the energies of the chromium 4s and 3d levels, especially, lie very close to those of boron 2p. In contrast to the case for CaB_6, where the calcium atom is just a source of two electrons, we need here to consider the details of the interaction of the metal and boron orbitals for CrB_4. In **8** we show the effect on the density of states

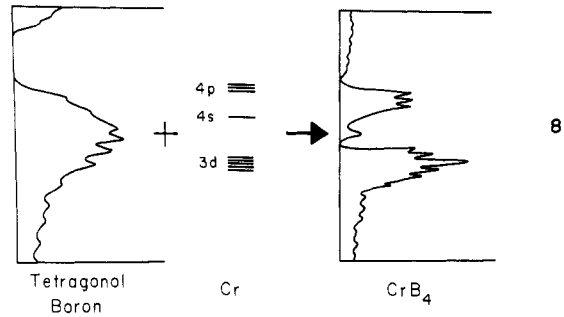

8

of "tetragonal boron" of adding a Cr atom to the non-metal framework. A large "bite" has been taken out of the valence band of this structure as a result of strong mixing between the Cr and B levels. The density of states for CrB_4 is shown in Figure 4a with an electron occupation appropriate to Cr. The result is rather a striking one, with the Fermi level located at a distinct minimum in the plot. Figure 4b shows the projection of the metal character from these levels. It is quite clear that the levels located around the Fermi level contain a large amount of metal character and, from Figure 4c, specifically a large amount of metal z^2 character.

We may understand how this collection of levels arises in the computed band structure by looking at the levels of a *molecular* fragment of stoichiometry MB_{12}. This unit will represent the immediate coordination environment of the metal. In such a fragment there will be many levels, largely located on the boron atoms, that will be involved in interactions with other atoms of

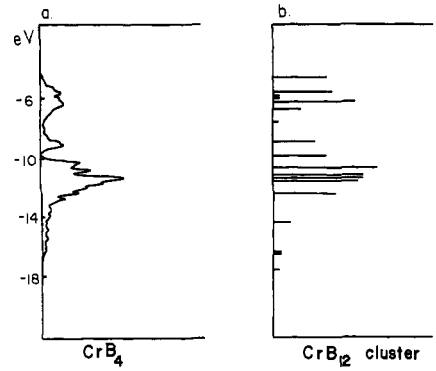

Figure 5. Projections of the Cr 3d orbitals from (a) the CrB_4 solid and (b) the CrB_{12} molecular cluster.

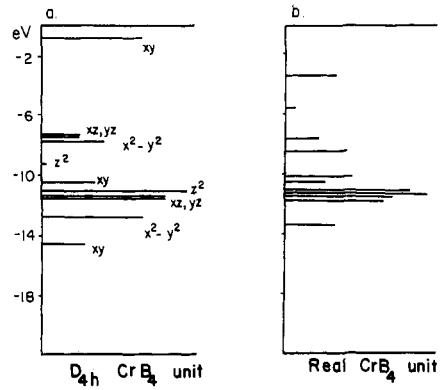

Figure 6. Projections of the metal 3d character for the (a) the ideal D_{4h} and (b) real CrB_4 "square" units.

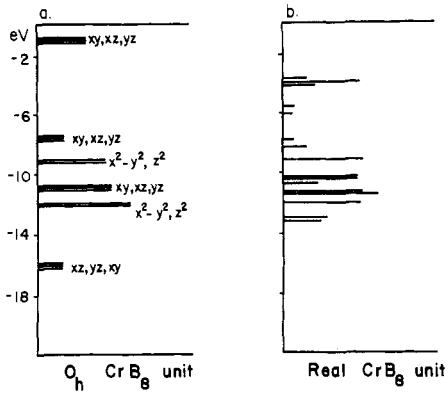

Figure 7. Projections of the metal 3d character for the (a) ideal O_h and (b) real CrB_8 "cubal" units.

the lattice. As a result, a conventional molecular orbital diagram is rather complex and hides the features we wish to see due to the presence of these spare orbitals. However, projection of the metal d character from such a diagram sidesteps this problem, gives us clues as to the origin of the partial density of states in Figure 4b, and hence gives information concerning the location of the Fermi level.

Figure 5 shows the result of such an analysis. The major features of the metal projected density of states of the solid match up quite nicely with those from the CrB_{12} cluster. A prominent feature is the separation into two sets of levels around the Fermi level both in the solid and in the molecule. We may in turn readily specify the origin of the relevant peaks in the density of states by projecting out the metal character from molecular orbital calculations on "square" CrB_4 and "cubal" CrB_8, two arrangements of potentially high symmetry that will allow us to understand where these levels have come from. Figures 6 and 7 show orbital diagrams for these two units and the result of lowering the symmetry (from O_h in CrB_8 and from D_{4h} in CrB_4) to that observed in the solid.

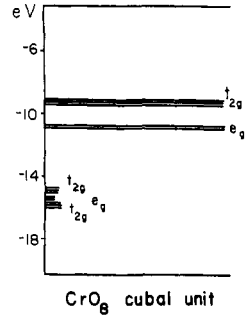

Figure 8. Projection of the metal 3d character for an ideal CrO_8 cubal unit.

For the square environment, the metal d orbitals transforms as $a_{1g} + b_{1g} + b_{2g} + e_g$. The xy and z^2 orbitals are involved in σ interactions with the ligands (**9**). The (xy,yz) pair and $x^2 - y^2$ orbitals are involved in π interactions. The diagram takes on an unconventional look in Figure 6a because the metal 3d levels are straddled by the boron 2s and 2p levels in energy. The transformation properties of the four 2s orbitals and the four 2p orbitals which point at the metal (σ) are identical (**9**). This leads to three entries in the density of states for xy, located at the top, bottom, and middle of the diagram. This is the strongest of the two σ interactions. Interaction with the collar of z^2 is weak, and most of the z^2 character is found in a single level close to that of the free metal d energy. π bonding between metal d and boron p orbitals is important, and bonding and antibonding pairs are produced. Notice that the orbitals lying closest to the unperturbed metal d levels are M–B π bonding, a direct consequence of having 2p orbitals that lie higher in energy than the metal d levels. As far as chromium is concerned, the boron atoms may be acting as electron acceptors, an interesting point we will return to. The general pattern of these levels is retained on distortion to the rectangular environment of the CrB_4 unit in the crystal.

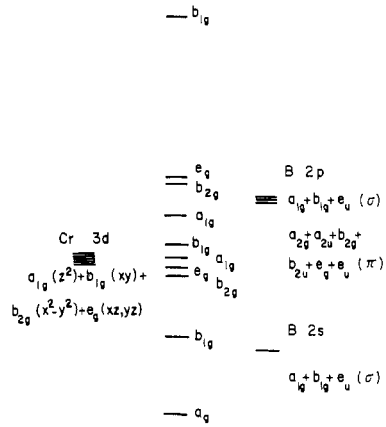

9

Figure 7 shows a similar pair of diagrams for the CrB_8 cube. Here the pattern is very simple as a consequence of the high symmetry of this unit and is easily understood (**10**). Notice that σ interactions are only associated with the t_{2g} representation, while π interactions are associated with both e_g and t_{2g} representations. σ–π mixing can and does occur here. The representations spanned by the B 2s orbitals contain t_{2g}, whereas those spanned by the B 2p orbitals contain e_g and t_{2g}. Thus, there will be four entries for the triply degenerate levels (t_{2g}) arising from B 2s(σ), B 2p(σ), B 2p(π), and Cr 3d. With this information the origin of the projections of Figure 7a is easy to see. What is quite striking is the almost equal importance of metal character in several of these levels such that it is impossible to consider a "normal" splitting pattern for such a system, as is traditionally done for transition-metal–ligand interaction diagrams. Consider especially the almost equal distribution of metal character in the two sets of levels of e_g symmetry. Figure 8 shows a plot analogous to that of Figure

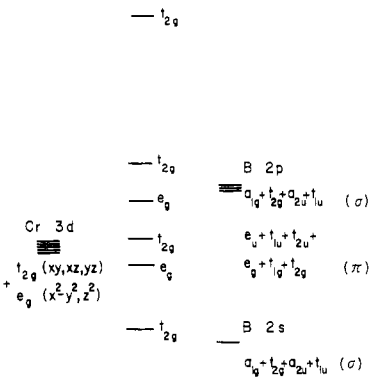

10

7a but for a cubal CrO_8 unit. The oxygen atom contains 2s and 2p levels that lie below the d orbitals of the metal, a more "normal" situation. Notice the relative weight of the metal character in the sets of orbitals and contrast this with the boron case. Notice too the characteristic d orbital splitting pattern for the cubal CrO_8 complex in the relevant energy region.

Distortion of the cube away from the ideal geometry to the one observed in the crystal splits the degeneracies, of course, but it is relatively easy to trace the parentage of the levels in the lower symmetry structure. Of particular interest to us is the change in the nature of the orbitals that lie around −9 eV. In the ideal cube there is a pair of levels that represent the M–B antibonding component of e_g symmetry associated with the metal $x^2 - y^2$ and z^2 orbitals. On distortion, the degeneracy is removed and the lower energy member becomes almost exclusively z^2. Figure 4c shows the z^2 projection for the crystalline solid, broadened into a band by interaction not only with boron but also with the adjacent metal atoms in the structure. The bottom of the band will be metal–metal bonding but, as the energy increases, will become increasngly metal–metal antibonding. The Fermi level for CrB_4 lies in the middle of this projected band. **11** shows the orientation of z^2

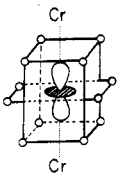

11

relative to the boron atoms of the coordination environment. An important point is that the levels just above the Fermi level for CrB_4 will be both metal–metal and metal–cubal boron antibonding (**10**).

V. Factors Influencing the Structure

Having seen where these energy levels come from, we are now in a position to be able to probe the electronic factors that could influence the stability of these MB_4 systems. Figure 9 shows the COOP curves for the three linkages of interest, M–B (square), M–B (cube), and M–M. These curves depict the bonding or antibonding behavior of the relevant linkage as a function of energy. Notice that for the vanadium electron count the M–B overlap population has reached a maximum (numerically 0.278) for the linkages within the square. For chromium a maximum (numerically 0.182) is reached for the corresponding cubal linkages. Extra electrons can only weaken these bonds, specifically the linkages to the cubal atoms suggested by the orbital analysis above. (However, as Table I shows, the cubal linkages are somewhat shortened in MnB_4 relative to those in CrB_4.) As far as metal–metal bonding is concerned, at the chromium electron count some M–M antibonding levels have been occupied such that the resulting overlap population is small but positive. With more electrons the metal atoms become repulsive.

Such a discussion suggests that the stabilization energy of an MB_4 species with this structure should be maximized at this

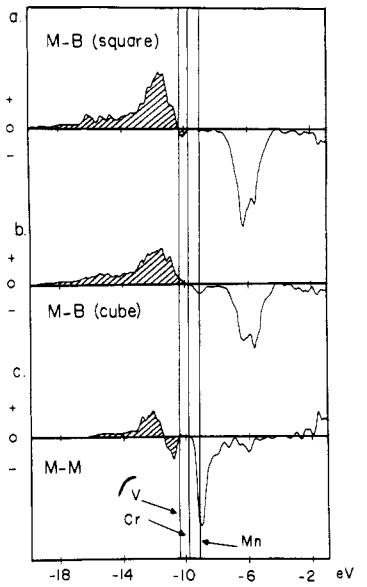

Figure 9. Crystal orbital overlap populations (COOP) for (a) the M–B (square), (b) the M–B (cube), and (c) M–M bonds of the CrB_4 structure. The shading corresponds to the electron count appropriate to Cr.

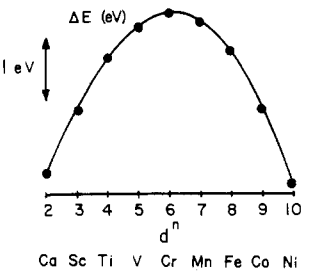

Figure 10. Computed variation with d count of the heat of formation of MB_4 borides with the CrB_4 structure. The abscissa has been labeled with the appropriate first-transition-series metals. (Numerically these values represent the energy of an MB_4 system with a given d count relative to (arbitrarily) ScB_4 and a free 3d electron.)

Table II. Charges on Metal Atoms in the CrB_4 Structure as a Function of Electron Count[a]

metal corresponding to d count	electrons at metal	electrons at boron
V	6.89	2.53
Cr	7.46	2.63
Mn	8.10	2.72
Fe	8.47	2.88
Co	8.77	3.06

[a] These figures have been obtained from calculations that used chromium parameters and the CrB_4 geometry. As the electronegativity of the metal increases (V–Co), these computed metal densities will be somewhat larger than a more realistic model would give for Mn–Co.

electron count. This is just what is found computationally. Figure 10 shows the computed stabilization energy variation with d electron count. The plot shows the variation relative to a species with an electron count appropriate to ScB_4 and a free metal d electron. Elsewhere we show[10] in more detail how a similar analysis leads to an excellent correlation with the experimentally determined heats of formation of AlB_2 type borides, where the maximum lies at M = Ti. There are no thermochemical data for these MB_4 species.

From the plots of Figure 9, without any knowledge of their origin, at the vanadium or chromium electron count the CrB_4 structure appears to be almost ideally arranged as far as the metal atom coordination is concerned. Although the actual numbers should be interpreted with caution, it is striking that, from Table

(10) Burdett, J. K.; Canadell, E.; Miller, G. *J. Am. Chem. Soc.* **1986**, *108*, 6561.

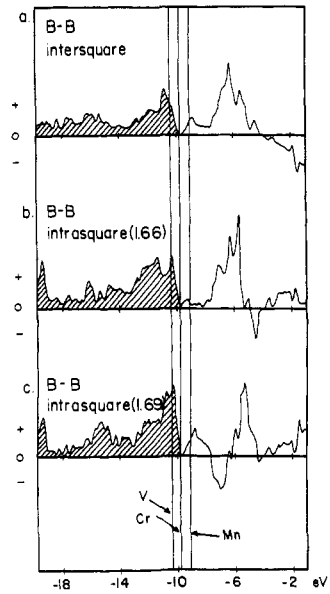

Figure 11. Crystal orbital overlap populations for the B–B bonds in the CrB_4 structure. The shading corresponds to the electron count appropriate for Cr.

II, for all the metals from V to Co there is transfer of electron density away from the non-metal net. In this respect the gross electronic picture is exactly opposite to that mentioned earlier for CaB_6, where donation occurs from metal to boron. When we return to our point concerning the stability of the non-metal net with electron count (Figure 2), the figures of Table II suggest that the net should be increasingly unstable on moving to the right of the transition-metal series. Direct correlation of the numbers from a population analysis of CrB_4 (shown in Table II) with the plot of Figure 2 we feel is inappropriate, but the qualitative trend is clear. We do note, however, that the increase in boron density on moving from M = Mn to Fe and from M = Fe to Co is significantly larger than that for M = Cr to Mn. This reflects the large metal (z^2) character at the Fermi level for Mn (Figure 4) and the heavy-metal–boron mixing at higher energies.

It is of course interesting to ask why the "ideal" structure is not found for the boron net in CrB_4. As Figure 2 shows for all the electron counts of interest, the "ideal" net with its long-sided squares is computed to be more stable than the observed variant. In fact the "ideal" CrB_4 structure is almost certainly not stable because of the very short M–B (square) distances that it demands. In order to conserve a Cr–B distance of 2.06 Å, the B–B distance in the "ideal" structure would have to be 1.99 Å, a figure that is certainly too large. For M = V the increase in the size of the metal compared to that of chromium surely must preclude the formation of such an MB_4 structure completely. Such size arguments have already appeared in this context.[3,4]

MB_4 species with electron counts appropriate for M = V, Cr appear to represent a situation with good M–B and M–M interactions, as well as give rise to a boron net in which the instability of the squares in the structure, traditionally associated with carbon chemistry, has been reduced by ensuring a low non-metal electron density.

VI. The Distortion in MnB_4

Why is the structure with M = Mn distorted? There are two parts of this problem. The first is what we might have predicted for the movement of the metal given the peak in the density of states at the Fermi level for MnB_4, and the second is the observed distortion of the squares to rectangles with little change in metal coordination. One of the rather interesting aspects of the distortion is that, for Figure 11, for electron counts appropriate for Cr and Mn no B–B antibonding orbitals are occupied. (At M = Fe some intrasquare antibonding orbitals are being occupied.) Why the system distorts to produce such large bond length changes by the simple addition of one electron per formula unit is then a particularly quizzical one.

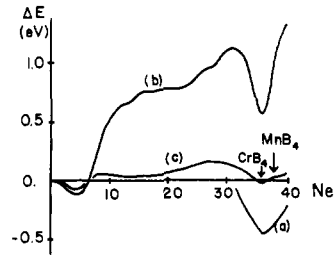

Figure 12. Computed variation with the electron count of the relative stabilities of the real CrB_4 structure and various alternatives: (a) distortion to **13**; (b) distortion to the real structure of MnB_4; (c) distortion to the "semi-MnB_4" structure, via a path that maintains orthorhombic symmetry and is less extreme than that of (b). See Appendix for details. When the curve is negative, the real CrB_4 structure is more stable.

From Figures 4 and 9 the M = Mn electron count results in a locally large density of states at the Fermi level with what appears to be half-occupation of a band largely metal z^2 in character. This situation is reminiscent of the situation in the undistorted parent of the platinum mixed-valence compounds **12**.

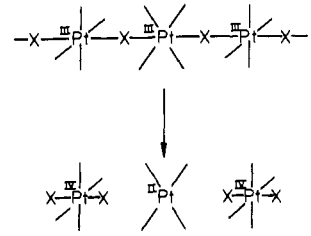

12

Here the presence of such a half-filled z^2 level signals a distortion to a system where the metal–bridging halogen distances are not all equal. In principle both a symmetric distortion (leading to the mixed-valence pair of species Pt(II) and Pt(IV) as shown in **12**) and an antisymmetric motion (leading to Pt(III)) are possible. We have performed calculations for a model distortion of the type shown in **13**. Here each metal atom is now surrounded by an

13

asymmetric array of cubal boron atoms. The results show (Figure 12, curve a) that the distortion is not favored at the chromium electron count but is stabilized for M = Mn. Overall, however, we find that for MnB_4 this is not favored energetically with respect to the observed monoclinic structure (Figure 12, curve b). Also shown are the results for the "semi-MnB_4" distortion. The distortion of the "squares" is not quite as large in this structure compared to that in MnB_4. Notice the sharp minima in these MB_4 stabilization curves at the chromium electron count and the relative stability of the MnB_4 geometry for electron configurations on either side.

We are not concerned about the failure of the computation to reproduce numerically the stability of the CrB_4 structure at the appropriate electron count. Calculations such as ours, as we have noted already, do not accurately reflect the energy differences between structures with different bond lengths. Since the average M–B distance is shorter in MnB_4 than in CrB_4 (see Table I), the former will have the larger second moment[9] and the computed stability curve will in general favor the MnB_4 structure. Notice the similarity of these curves to those of Figure 3. The effect of the metal has been to "stretch" the abscissa, and commensurate with this variation in second moment has given the plot an apparent upward slope. Although out orbital method does not do

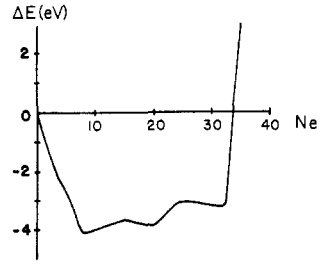

Figure 13. Computed energy difference curve for the non-metal net alone for the breakup of the CrB_4 structure via distortion to the RuB_2 structure. A negative value means that the CrB_4 structure is more stable.

Table III. Parameters and Exponents Used in the Calculations

atom	orbital	H_{ii}, eV	ζ_1	ζ_2	c_1[a]	c_2
B	2s	−15.20	1.30			
	2p	−8.50	1.30			
C	2s	−21.40	1.625			
	2p	−11.40	1.625			
O	2s	−32.30	2.275			
	2p	−14.80	2.275			
Cr[15]	4s	−8.66	1.70			
	4p	−5.24	1.70			
	3d	−11.20	4.95	1.80	0.5058	0.6747

[a] Contraction coefficients used in the double-ζ expansion.

a very good job of weighting the energetics invovled in these bond-length distortions, it lends support to the idea of a distorted structure for MnB_4. Recall the quoted errors in the experimentally determined crystal structure[4] are high.

We noted earlier that the distortion in MnB_4, carried to an extreme, would lead to an RuB_2 type of non-metal net. Are structures of this type possible ones for CrB_4? Figure 13 shows a computed energy difference curve for this geometrical change for the non-metal net alone.[11] Only at electron counts past the half-filled band does this become a possibility. An exactly analogous structural change is that[5] of the breakup of the hexagonal diamond structure (with eight electrons per atom pair) to give that of GaS or that of wolfsbergite (with an average of nine electrons per atom pair). Such gross structural changes are only predicted for electron counts much greater than those we find here. In other words, defect AlB_2 type structures with the MB_4 stoichiometry should not be viable structural alternatives at these electron counts. Many more electrons are needed before B–B antibonding levels can be populated such that these linkages can be broken.

It is difficult to accurately pinpoint the reasons for the CrB_4 to MnB_4 distortion. However, we can devise a picture that is in accord with our results and discussion above. The COOP curves tell use that all B–B linkages should strengthen as the electron count increases but that M–M and M–B (cubal) linkages should weaken. This is clearly impossible to achieve geometrically because in the orthorhombic cell, if all B–B distances shorten, the M–M and M–B distances must shorten too. We note that the largest single change in overlap population occurs between the metal atoms. (This changes from a positive to a negative value.) The structural change that occurs on moving from M = Cr to Mn is then a direct result of the relief of severe metal–metal antibonding interactions. The MnB_4 arrangement is one that contains much reduced metal–metal interactions but is also one that takes advantage of the instability of the non-metal net at the boron count as we discussed extensively in section II. The metal–metal interactions are both through-space and through-bond. The distortion **13** is less energetically favored since only the latter interactions are relieved here.

There are some sites (those of (2b)) in the structure of CrB_4 that remain empty. These eighth-coordinate interstices are just the right size for occupation by a first-row atom, such as another boron for example. It would be an extremely useful test of our claim for strong electronic control of this structural problem if doped CrB_4 systems could be made where the electron count could be varied around the V, Cr, Mn region. Useful too would be a study, such as XPS, on these two borides that would probe the electronic environment at the metal.

Acknowledgment. We thank the donors of the Petroleum Research Fund, administered by the American Chemical Society, for their support of this research. It was also supported by the National Science Foundation (NSF Grant No. DMR8414175). J.K.B. thanks the Laboratoire de Chimie Théorique de l'Université de Paris-Sud, Orsay, France, for hospitality when some of this research was performed and Gordon Miller for a very useful conversation.

Appendix

The calculations are of the extended Hückel type[12,13] with the parameters and exponents of Table III. The modified Wolfsberg–Helmholz formula[14] was used. Structural details for use in the calculations on CrB_4 and the different molecular fragments were taken from the experimentally determined structures.[3,4] The B–B distance used in the computations on tetragonal boron was 1.80 Å, and the angles external to the square were set at the tetrahedral angle. Calculations on cubic and tetragonal carbon employed a C–C distance of 1.54 Å. The cell dimensions of the orthorhombic structure described as "semi-MnB_4" were the same as those for the observed CrB_4 structure, but the atomic coordinates of the boron atoms were such that the rectangular distortions of the B_4 squares were half as large as in the real MnB_4 structure. The model distortion shown in **13** used a displacement of the metal atoms by 0.1 Å compared to the positions in the real CrB_4 structure. Calculations routinely employed a set of 64 k-points within the irreducible wedge of the orthorhombic Brillouin zone.

Registry No. CrB_4, 12409-08-4; MnB_4, 12271-96-4.

(11) The general shape of this curve is also influenced by the coordination number problem, described in terms of a second moment above. Since the coordination number is larger in the CrB_4 structure than in the RuB_2 arrangement, the former is computed to be overwhelmingly stabilized on our one-electron model for low electron counts.

(12) Hoffmann, R. *J. Chem. Phys.* **1963**, *39*, 1397.
(13) Whangbo, M.-H.; Hoffmann, R. *J. Am. Chem. Soc.* **1978**, *100*, 6093.
(14) Ammeter, J. H.; Bürgi, H. B.; Thibeault, J.; Hoffmann, R. *J. Am. Chem. Soc.* **1978**, *100*, 3686.
(15) Summerville, R. H.; Hoffmann, R. *J. Am. Chem. Soc.* **1976**, *98*, 7240.